

Phase Evolution of the Crab Pulsar between Radio and X-ray

L.L. Yan^{1,2,3}, M.Y. Ge¹, J.P. Yuan⁴, S.J. Zheng¹, F.J. Lu¹, Y. L. Tuo^{1,2}, H. Tong⁴, S.N. Zhang¹, Y. Lu¹, J.L. Han⁵, Y.J. Du³

¹Key Laboratory of Particle Astrophysics, Institute of High Energy Physics, Chinese Academy of Sciences, Beijing 100049, China; yanlinli@ihep.ac.cn

²University of Chinese Academy of Sciences, Beijing 100049, China.

³Qian Xuesen Laboratory of Space Technology, No. 104, Youyi Road, Haidian District, Beijing 100094, China

⁴Xinjiang Astronomical Observatory, Chinese Academy of Sciences, Urumqi, Xinjiang 830011, China

⁵National Astronomical Observatory, Chinese Academy of Sciences, Jia 20 Datun Road, Beijing 100012, China

Received _____; accepted _____

ABSTRACT

We study the X-ray phases of the Crab pulsar utilizing the 11-year observations from the *Rossi X-ray Timing Explorer*, 6-year radio observations from the Nanshan Telescope, and the ephemeris from Jodrell Bank Observatory. It is found that the X-ray phases in different energy bands and the radio phases from Nanshan Telescope show similar behaviors, including long-time evolution and short-time variations. Such strong correlations between the X-ray and radio phases imply that the radio and X-ray timing noises are both generated from the pulsar spin that cannot be well described by the the monthly ephemeris from the Jodrell Bank observatory. When using the Nanshan phases as references to study the X-ray timing noise, it has a significantly smaller variation amplitude and shows no long-time evolution, with a change rate of $(-1.1 \pm 1.1) \times 10^{-7}$ periods per day. These results show that the distance of the X-ray and radio emission regions on the Crab pulsar has no detectable secular change, and it is unlikely that timing-noises resulted from any unique physical processes in the radio or X-ray emitting regions. The similar behaviors of the X-ray and radio timing noises also imply that the variation of the interstellar medium is not the origin of the Crab pulsar’s timing noises, which is consistent with the results obtained from the multi-frequency radio observations of PSR B1540–06.

Subject headings: stars:neutron — pulsars: individual (PSR B0531+21) — X-rays:
stars

1. Introduction

Pulsars are famous for their rotation stability and highly repeatable pulse shapes. However, when examining pulsar’s periodicity with high precision, there appear to be two main types of irregularities, namely glitch and timing noise. The origin of timing noise remains controversial in spite of years of studies. Models proposed to explain the timing noises of pulsars include the random process (Cordes and Helfand 1980), unmodeled planetary companions (Cordes 1993), the free precession (Stairs et al. 2000), and the interstellar medium (ISM; e.g. You et al. (2007)). Hobbs et al. (2010) analyzed the timing properties of 366 pulsars in detail. Their study shows that timing noise is widespread in pulsars and cannot be explained using a simple random walk in the observed rotational parameters. The timing residuals of PSR B1540–06 are consistent at different radio frequencies, which implies that its timing noise is not caused by ISM (Hobbs et al. 2010). The underlying physical processes that cause timing noise are still unclear.

Among all the pulsars, the Crab pulsar is probably the most suitable source to study the origin of timing noise for its frequent spin irregularities and abundant observational data. This pulsar has been comprehensively studied in almost all wavelength bands from radio to very high energy γ -rays. Its pulse profile shows a double-peak structure in all of these wavebands. Generally, the two dominant pulses in the radio band are denoted as main pulse (MP) and interpulse (IP; Lyne et al. (2013)), and the two X-ray peaks are denoted as P1 and P2 (Kuiper et al. 2001). Detailed studies show that the exact pulse morphology varies as a function of photon energy (Abdo et al. 2010; Ge et al. 2012) and the positions of the main peak in different energy bands are not exactly aligned, i.e., the optical, X-ray and γ -ray pulses lead to the radio pulses (Kuiper et al. 2003; Rots et al. 2004; Oosterbroek et al. 2008; Abdo et al. 2010; Molkov et al. 2010). Recently, secular changes of both the radio and the X-ray profiles were found, though their change rates are different from each other

(Lyne et al. 2013; Ge et al. 2016). These changes were attributed to a progressive change in the magnetic inclination (Lyne et al. 2013; Ge et al. 2016), and such magnetic field variations are also confirmed by another study on red timing noise (Yi and Zhang 2015). With seven years of observations, it was found that the X-ray pulse in 2–16 keV leads the radio one by 0.0102 ± 0.0012 period and increases with a rate of $(3.3 \pm 2.0) \times 10^{-7}$ period per day (Rots et al. 2004), which could also be explained as systematic errors. Given the secular changes of the radio and X-ray profiles, to study the phase lags between different energy bands and their variations is important to uncover the origin of timing noise and the properties of magnetosphere structure.

In this paper, by using the 11-year observations from the *Rossi X-ray Timing Explorer (RXTE)*, 6-year radio observations from Nanshan radio telescope at the Xinjiang Astronomical Observatory (Wang et al. 2001), and the monthly renewed ephemeris from the Jodrell Bank Observatory (Lyne et al. 1993), we investigated in detail the timing behaviors of this pulsar in the X-ray and radio wavebands. First, the phase comparisons between the Proportional Counter Array (PCA) and the High Energy X-ray Timing Experiment (HEXTE) on board *RXTE* are used to estimate the instrumental influences on the phase determination. Then, the accuracy of the Jodrell Bank ephemeris is checked by the correlation between the X-ray phases and the radio phases obtained by the Nanshan radio telescope. Furthermore, the X-ray phases are corrected by the new phase indicator from Nanshan radio telescope to study the relationship between the X-ray and radio timing noises, including the effects of the dispersion measure (DM).

2. Observations and Data Reduction

2.1. Timing Ephemeris from Jodrell Bank

In this study, the time reference for the radio phases from Nanshan and X-ray phases from *RXTE* of the Crab pulsar is taken as the times-of-arrival (TOAs) from Jodrell Bank radio ephemeris (JBE; Lyne et al. (1993)). A 13 m radio telescope at Jodrell Bank monitors the Crab pulsar daily, offering a radio ephemeris ¹ that is used for the analyses of *RXTE* and Nanshan data. The ephemeris we used is in CGRO format, the format required by the *RXTE* data processing, and it contains the following information: R.A. and decl. in J2000 coordinates, the first and last dates for valid parameters, the infinite-frequency geocentric UTC TOA of a pulse, rotation frequency and its first two derivatives, the barycentric (TDB) epoch of the spin parameters, and the root-mean-square radio timing residual. Because of the uncertainties of the radio receiver system and the calibration, we add a systematic error of $40 \mu\text{s}$ for phases calculated from this ephemeris as suggested by Rots et al. (2004). All errors of the phases in this paper are 1σ , for both statistical and systematic errors.

2.2. *RXTE* Observations and Data Reduction

The X-ray observations used in this paper were obtained by both PCA and HEXTE on board the *RXTE*. The PCA instrument is composed of five Proportional Counter Units with a total photon collection area of 6500 cm^2 . Its effective energy range is 2–60 keV, and the time resolution is about $1 \mu\text{s}$ (in Good Xenon mode; Jahoda et al. (2006)). These properties make PCA an ideal instrument to study the detailed temporal properties of pulsars. In this paper, we use the publicly available data in event mode E_250us_128M_0_1s. The time

¹<http://www.jb.man.ac.uk/pulsar/crab.html>

resolution of this mode is about $250 \mu\text{s}$. HEXTE consists of two independent detector clusters A and B, and each of them contains four NaI(Tl)/CsI(Na) scintillation detectors. This instrument is sensitive in 15–250 keV, with a detection area of 1600 cm^2 and a time resolution of $7.6 \mu\text{s}$ (Rothschild et al. 1998). In its default operation mode, the field of view of HEXTE, each cluster is switched on and off source to provide instantaneous background measurements. The HEXTE data used in this paper are in mode E_8us_256_DX0F.

The PCA and HEXTE data were analyzed by using the FTOOL from the astronomy software HEASOFT (v6.15). The method of data reduction and pulse profile calculation is the same as in Ge et al. (2016), but with the observations selected a little differently. Only 243 observations between MJD 51955 (2001 February 15) and 55927 (2012 January 01) are used in this paper, since from each of these observations high statistical PCA and HEXTE pulse profiles can be obtained simultaneously. The pulse profiles were binned into 1000 phase bins, in energy bands 2–60 keV for PCA and 15–250 keV for HEXTE.

2.3. Nanshan Radio Telescope Observations and Data Reduction

The Nanshan 25 m radio telescope, operated by Xinjiang Astronomical Observatory, started to observe the Crab pulsar frequently in 2000 January. As described in Wang et al. (2001), the two hands of circular polarization at 1540 MHz are fed through a $2 \times 128 \times 2.5$ MHz analogue filter bank. The signal is sampled at 1 ms intervals and 1 bit digitized. Time is stamped by a hydrogen maser calibrated with the Global Position system. The integration time of each observation of the Crab pulsar is 16 minutes. After 2010 January, the data were obtained with digital filter bank 3 (DFB3), which was configured to a bandwidth of 0.5 MHz for each sub-channel and 8 bit sampling. The data are folded online with a subintegration time of 1 minute for AFB and 30 s for DFB3, and then written to the disk with 256 bins across the pulse profile for AFB and 512 bins for DFB.

As for the radio observations, the off-line data reduction is performed in the following three steps by using the PSRCHIVE package: (1) the data for the Crab pulsar are de-dispersed using the DM values from the JBE timing results and then summed to produce a total intensity profile; (2) local TOAs were determined by correlating the data with standard pulse profiles of high signal-to-noise ratio, and the pulse TOAs normally correspond to the peak of the main pulse; (3) convert TOAs to the solar system barycentre. The detail data reduction process is the same as in Yuan et al. (2010). Because the data quality is better after 2005 May, we only analyzed those from MJD 53500 (2005 May 10) to 55688 (2011 May 07), and finally got 524 TOAs at 1540 MHz.

3. Phase Calculation and the Linear Fitting Method

3.1. Phase Calculation for *RXTE*

As described in Ge et al. (2012), the two asymmetrical pulses of the Crab pulsar in the X-ray band could be modeled by the formula (1) proposed by Nelson et al. (1970). In this paper, we only fitted the shape of P1 of the X-ray profile to obtain its peak phase.

$$L(\phi - \phi_0) = N \frac{1 + a(\phi - \phi_0) + b(\phi - \phi_0)^2}{1 + c(\phi - \phi_0) + d(\phi - \phi_0)^2} e^{-h*(\phi - \phi_0)^2} + l, \quad (1)$$

where L is the intensity at phase ϕ , l is the baseline of the light curve, ϕ_0 is the phase shift, N is the pulse height of the profile, and a , b , c , d and h the shape coefficients. The pulse phase is measured in phase units, of range (0,1). We fitted the shape of P1 with a relatively broad phase window (−0.055, 0.0355) centered at phase −0.01.

The calculation procedures of phases of P1 and the estimation of their statistical errors are the same as in Ge et al. (2012). The X-ray phases with high precision are obtained after the fitting procedure, and we denote the phases of the X-ray pulse P1 as Φ_P , Φ_H for PCA and HEXTE, respectively.

3.2. Phase Calculation for Nanshan

The calculation procedures of the radio phase of MP for Nanshan (Φ_N) are as follows:
 (1) Remove the dispersion effect for TOAs using the DM values from JBE (Lyne et al. 1993). In this step, we need to reckon the DM values in Nanshan observations using linear interpolation. The time delay (t_{DM}) caused by DM is

$$t_{\text{DM}} = D \times \frac{\text{DM}}{\nu^2}, \quad (2)$$

where D is the dispersion constant, $D = 4.1488 \times 10^3 \text{ MHz}^2 \text{ pc}^{-1} \text{ cm}^3 \text{ s}$, and ν is the centered frequency, i.e. 1540 MHz (Lyne and Graham-Smith 2012). Because the JBE DM values were not obtained in the same time as the Nanshan observations, the DM at the time of Nanshan observations were obtained with linear interpolation. (2) Convert the TOAs from Jodrell Bank and Nanshan to the TDB time system. (3) Calculate ϕ_J for Jodrell Bank and Φ_N relative to ϕ_J with formula (3) and (4), respectively.

$$\phi_J = f_0(T_J - T_0) + \frac{1}{2}f_1(T_J - T_0)^2 + \frac{1}{6}f_2(T_J - T_0)^3, \quad (3)$$

$$\Phi_N = \text{mod} [f_0(T_N - T_0) + \frac{1}{2}f_1(T_N - T_0)^2 + \frac{1}{6}f_2(T_N - T_0)^3 - \phi_J, 1], \quad (4)$$

where T_J and T_N are the TOAs in the TDB time system, from Jodrell Bank and Nanshan, respectively, f_0 , f_1 and f_2 are the spin parameters at the reference epoch T_0 , and mod is to obtain the residual after removing the integral periods. The final errors of Φ_N are from the errors of Nanshan TOAs and the systematic uncertainty of 40 μs as mentioned previously. In order to investigate the effect of DM on the timing noises, we also calculate the Nanshan phases without de-dispersion by skipping the first step above, and denote it as Φ_{N_0} . Because of the process “mod”, i.e. removing the integral periods, the difference of Φ_{N_0} and Φ_N is smaller than one period (see Fig. 4).

3.3. Methods for Phase Analysis

3.3.1. Linear Fitting

In order to study the phase variations versus time and the correlations between phases from different data sets, we fit the data points with a linear function. For the variation of a parameter versus time, if the slope deviates significantly from zero, long-term evolutions should exist. For the correlations between two parameters, the slope can also tell us information about how these two parameters are correlated, as we will discuss in section 4.

In this paper, the fitting method is the robust linear modeling (RLM) from the R statistical software package (Feigelson and Babu 2012), which has been used to study both the phase variations versus time and the correlations between different phases. The *MASS* (Modern Applied Statistics with S) library based on R-language has the *rlm* function for RLM. In this function, the fitting is achieved using an iteratively reweighted least-square algorithm. Similarly, the linear fitting for the phase correlations between different data groups is also achieved by this method, as listed in Table 1 and Table 2.

3.3.2. Correlation Analysis

The Pearson’s correlation coefficient r (Lee Rodgers and Nicewander 1988) is a suitable parameter to describe the influence of the timing noise on Φ_P , Φ_H and Φ_N quantitatively. Because the Nanshan and RXTE observations were not done simultaneously, and the time series of Φ_N is serially dependent when checking the autocorrelation function, the Nanshan phases at the time of X-ray observations (Φ'_N) are computed by linear interpolation between the neighboring Φ_N values.

4. Results

The X-ray phases Φ_P and Φ_H are the phases of the X-ray main peaks relative to JBE, from the PCA and HEXTE data respectively. In order to study the relation of the radio and X-ray phases on both long and short time scales, we need to check the accuracy and reliability of these phases first.

4.1. The X-Ray Phases from PCA and HEXTE and Their Correlation

As shown in Fig. 1, the X-ray phases Φ_P and Φ_H exhibit simultaneous variations on all time scales. Previous work showed that the X-ray phases from PCA gradually increase with a change rate of $(3.3 \pm 2.0) \times 10^{-7}$ period per day (MJD 50129–52941, Rots et al. (2004)) or $(6.6 \pm 1.3) \times 10^{-7}$ period per day (MJD 51955–55142, Ge et al. (2012)). Here we analyze more observations, in a longer time range MJD 51955–55927, and both PCA and HEXTE showed the same trend with the change rates of $(5.0 \pm 0.9) \times 10^{-7}$ and $(4.5 \pm 0.9) \times 10^{-7}$ period per day, respectively. Besides the increasing trends, Φ_P and Φ_H have two kinds of variations on short time scales, which are the slow variations (e.g. in MJD 52600–53000 and 55000–55200) and phase jumps (three points around MJD 53350, corresponding to the JBE in one month).

Correlation coefficient is calculated to estimate the degree of correlation between Φ_P and Φ_H . As shown in Fig. 2 and listed in Tab. 2, Φ_H is almost proportional to Φ_P , with a slope of 0.98 ± 0.02 and the Pearson’s coefficient $r = 0.96$, which means that they vary synchronously with the same amplitude. The synchronous variations between Φ_P and Φ_H imply that they have the same origin.

4.2. The Correlation between X-Ray and Nanshan Phases

The Nanshan radio phases Φ_N are also obtained by using the same JBE, and they show variations in different time scales too, as illustrated in Fig. 1e and Fig. 3a. Compared with Φ_P in the same time range, Φ_N shows similar fluctuations, especially in MJD 55000–55200 as in the zoomed in Fig. 3b. For the secular change, Φ_N increases linearly with a change rate of $(6.3 \pm 1.0) \times 10^{-7}$ period per day in MJD 53500–55688, which is consistent with the change rate Φ_P , $(4.8 \pm 2.1) \times 10^{-7}$ period per day in the same time range. These two change rates were obtained in a relatively short period are also consistent with the results obtained from the whole time range for Φ_P and Φ_H . As shown by the cross marks in Fig. 2, Φ'_N and Φ_P exhibit a strong linear correlation, with the Pearson’s coefficient $r = 0.78$ (Tab. 2) and a slope of 0.72 ± 0.04 . The strong correlation between Φ'_N and Φ_P means that Φ_N and Φ_P also have a strong correlation.

The fitted slope between Φ_N and Φ_P (0.72 ± 0.04) is different from 1, the expected values of Φ_N and Φ_P have the same variation amplitude and an exactly linear correlation. One may think that there is some physics behind this. Nonetheless, we realized that this result probably originated from the data handling process. Since the X-ray and Nanshan radio observations are carried out in different times, we obtained the Nanshan phases at the time of X-ray observations with linear interpolation (Φ'_N), so as to study their correlation. This linear interpolation will reduce the amplitudes of the radio timing noises, and the larger the amplitude is, the bigger the fraction of the variation that will be reduced. As a result of this linear interpolation process, the slope can be smaller than 1.

If the JBE can describe the spin of the Crab pulsar accurately, Φ_N should be constant over time, because Φ_N is also inferred from the radio data. However, as given above, Φ_N has a secular change with a significance of nearly 6.3σ , and both its long-time and short-time variations are similar to the X-ray ones that are also derived from the JBE. It is very likely

that the temporal behaviors of the Crab pulsar cannot be accurately described by those spin parameters in the JBE, which also causes the apparent variation of the X-ray to radio phase lags.

4.3. The X-Ray Phases by Using the Nanshan Radio Ephemeris

The simultaneous secular changes and fluctuations of the X-ray and Nanshan radio phases imply that they may be caused by the timing noise of the Crab pulsar or the inaccuracies in the JBE. In order to further check the relations between the X-ray and radio phases, here we use the Nanshan phases Φ'_N as the phase references, and obtain the corrected X-ray phases Φ'_P from PCA data, which has a lower variation amplitude (i.e. standard deviation) 0.0013 compared to 0.0020 of Φ_P as shown in Fig. 3c. Moreover, Φ'_P keeps almost constant over the time range MJD 53500–55693 with a change rate of $(-1.1 \pm 1.1) \times 10^{-7}$ period per day. The disappeared secular change of the new X-ray phases suggests that the JBE is inaccurate.

5. Origin of the Phase Variation and Timing Noise

There are several factors that can result in the variabilities of the observed X-ray phases: the instability of the time system, the change of the instrument response, the timing noise of the pulsar, the inaccuracies of the ephemeris, and the intrinsic variation of the X-ray emitting region relative to the radio ones. The effects of these factors are discussed in the following.

5.1. Time System and Instrument Response

The Mission Operations Center of *RXTE* performs clock calibrations several times a day, using the User Spacecraft Clock Calibration System method, and the timing accuracy was improved from 4.4 to 2.5 μs on 1997 April 29 (Jahoda et al. 2006). Besides, the instrumental delay correction for the PCA is 16–20 μs and for the HEXTE it is 0–1 μs . The barycenter corrections by FTOOL has an accuracy of better than 1 μs and has also subtracted 16 μs to account for the instrumental delay in the PCA.² Therefore, the maximum timing uncertainties is $\sqrt{2.5^2 + 1^2} + 4 = 6.7 \mu\text{s}$, which has a much smaller impact on the timing measurement for X-ray photons than the 40 μs systematic error from JBE (Rots et al. 2004).

If the time systems of *RXTE* and the Nanshan telescope were inaccurate, wrong timing recorders would be assigned and thus would cause the abnormal phases. For PCA and HEXTE, the consistent variations might have been caused by the irregularity of the time system because they use the same time information from the satellite³. However, considering that Φ_P and Φ_N have very similar variations and they are based on two independent time systems, the inaccuracy of the time systems cannot account for the observed phase fluctuations.

The aging of detectors would also have impacts on the timing recorders. As the X-ray phase lag of the Crab pulsar evolves with energy (Molkov et al. 2010; Ge et al. 2012), the phase lag will change if the detection efficiency curve varies due to the instrument aging or other factors (Garcia et al. 2014). However, the change of the response functions of the X-ray instrument cannot explain the correlation between Φ_P and Φ_N , because the detectors

²<http://heasarc.gsfc.nasa.gov/docs/xte/abc/time.html>

³http://heasarc.nasa.gov/docs/xte/time_news.html

are totally different.

5.2. Inaccuracies in JBE

The inaccuracy in the ephemeris have direct impacts on the phase calculations for the X-ray and Nanshan phases. The effect of ISM, pulsar proper motion, glitches, as well as timing noises could all generate inaccurate parameters.

5.2.1. Effect of the ISM

Because of the existence of ISM, the arrival time of radio pulses is dependent on frequency. Both the mismeasurement of DM and the scattering of ISM have an impact on radio observations and phase results.

During MJD 55050–55350, the variation amplitudes of DM are larger than in the other time periods, which is apparently consistent with the questionable points in this time range. The phase change caused by DM could be obtained using $\Phi_{N0}-\Phi_N$, and its impact on the Nanshan phase could be evaluated by comparing it with Φ_N . However, as shown in Fig. 4, the phase change caused by DM is smaller than the phase fluctuation in both X-ray and Nanshan phases in MJD 55050–55350, as the DM effect has been removed in the JBE (Lyne et al. 1993). So, the large fluctuation in the X-ray and Nanshan phases in MJD 55050–55350 could not be explained by the DM effects.

As for the scattering of ISM, its influence on TOA could be evaluate by the following formula (Lyne and Graham-Smith 2012).

$$t_{\text{scatt}} = \left(\frac{\text{DM}}{1000}\right)^{3.5} \left(\frac{400}{\nu_{\text{MHz}}}\right)^4 \quad (5)$$

For the Crab pulsar, $\text{DM} = 56.78 \text{ pc cm}^{-3}$, and when $\nu_{\text{MHz}} = 1540 \text{ MHz}$ (Nanshan radio

band), $t_{\text{scatt}} \simeq 0.2 \mu\text{s}$. In the X-ray band t_{scatt} would be much smaller. It is thus clear that the influence of ISM scattering on the Nanshan and X-ray phases could be disregarded.

5.2.2. *Effect of the Proper Motion*

With accurate measurement by the Hubble Space Telescope, the proper motion of the Crab pulsar has been obtained as $\mu_\alpha = -11.8 \text{ mas yr}^{-1}$ for R.A. and $\mu_\delta = 4.4 \text{ mas yr}^{-1}$ for decl. (Kaplan et al. 2008). However, the JBE uses a constant position for the Crab pulsar, and the influence of proper motion on the relative phases should be considered. If the pulsar position is changing, the timing residuals should show oscillations with gradually increasing amplitude (Helfand et al. 1977), which could be roughly described by $\Delta\Phi_{pm} = h \cdot \sin \alpha \cdot \Delta\theta/c_0 \cdot f$, where h is the distance between the Earth and the Sun, c_0 is the speed of light, and α is the decl. of the Crab pulsar. Taking into account the proper motion, the maximum value of the amplitude is 0.0035 periods for 10 years. However, the impact of proper motion is counteracted when the time is longer than one month, because the X-ray and Nanshan phases are the relative phases to JBE that were updated monthly. We check the power spectrum of these relative phases to see whether variation power exists on the time scale of about a month, which could be the impact of pulsar proper motion on the relative phases, and eventually no significant signals in the power spectrum of Φ_P and Φ_H have been found. Thus, the proper motion is not the main reason for the long-term variation of the X-ray and Nanshan phases. Similarly, the inaccuracy of solar system ephemeris could not account for the long-term variation of the X-ray phases.

5.2.3. Check of the Spin Parameters

Inaccurate spin parameters could lead to phase deviation. There are some outliers in X-ray and Nanshan phases, especially the X-ray phases around MJD 53350, which are obtained by using one ephemeris. These results remind us to check the reliability of the JBE parameters, from the aspects of glitches, rotation frequencies, and radio reference TOAs.

Because the parameters of glitches have not been included in the JBE directly (Lyne et al. 1993), we need to check whether the significant residuals are caused by the glitches. However, we find that the obviously abnormal phases are not coincident with the glitch epoches. The effects of glitches after their occurrence month are greatly reduced. In MJD 53341–53372, there is no glitch, so the outliers in this period did not result from glitches.

Furthermore, we check the parameters of JBE in MJD 53341–53372 in case the JBE parameters are inaccurate. First, we compare the rotation frequencies inferred from JBE and those we searched from the three *RXTE* observations in this period. The maximal difference between them is $(0.3 \pm 1.2) \times 10^{-5}$ Hz for PCA and $(2.0 \pm 5.8) \times 10^{-5}$ Hz for HEXTE, where the uncertainties are only from our frequency searching process, which show that the frequencies we calculated from these three observations are consistent with the JBE predictions. Second, we calculate the TOAs of these three X-ray observations using the frequencies we obtained above and the software TEMPO2 (Edwards et al. 2006; Hobbs et al. 2006), and then compare them with the TOAs inferred from the JBE time solution and the FTOOL command FASEBIN. As shown in Fig. 1, TOAs obtained with the above two methods are consistent. Therefore, both the JBE frequencies and the TOA calculation process are reliable, and the remaining possibility is that the reference TOA of JBE in MJD 53341–53372 is inaccurate, which causes the abnormal lags between the X-ray and radio phases. We note that the inaccuracy of JBE TOAs has also been found by the

Jodrell Bank Observatory, as on the web page of JBE it is pointed out, “DO NOT trust the geocentric pulse arrival times yet!”⁴.

5.3. Is There a Significant Intrinsic Variation of the X-Ray Emitting Region Relative to the Radio Ones?

It is important for pulsar physics to find out whether the fluctuations and long-term evolutions of the X-ray phases are intrinsic, i.e., due to the relative geometric variations between the X-ray and radio emitting regions. We find that there are two observational facts contradicting with this hypothesis. As shown in Fig 2, the Nanshan radio phases are highly correlated with the X-ray phases derived from the PCA observations, which means that the two phases wander simultaneously. Furthermore, by using the Nanshan phases as a reference, the X-ray phases then have a smaller fluctuation amplitude and the long-term evolution disappears (Fig. 3c), which also implies that the X-ray and radio emitting regions do not have significant relative changes. Thus, the X-ray and radio phase fluctuations are both dominated by the pulsar spin.

5.4. Constrains on timing noises

The almost constant phase-lag between the X-ray and radio bands also supplies information about the origins of timing noises. Variations of the DM and thus the variations of ISM between the earth and pulsars have been detected, which can lead to the radio timing noises of those pulsars (You et al. 2007, and references there in). However, because the ISM has no effect on the X-ray TOAs, the constant value of the X-ray phase Φ'_P means

⁴<http://www.jb.man.ac.uk/pulsar/crab.html>

that most of the timing noises are not from the ISM, which is consistent with the results of PSR B1540–06 obtained from the multi-frequency radio observations (Hobbs et al. 2010). Thus ISM variation cannot account for all the timing noises of the Crab pulsar.

6. Summary

Utilizing the 11-year X-ray observations from the RXTE, 6-year radio observations from Nanshan Telescope, and the ephemeris from the Jodrell Bank Observatory, we study the evolution of the X-ray and radio phases of the Crab Pulsar. The X-ray phases from PCA and HEXTE exhibit synchronous variations on all time scales, and X-ray and Nanshan phases also have a strong correlation with a Pearson’s coefficient $r = 0.78$. We find that the simultaneous secular changes and fluctuations of the X-ray phases Φ_P , Φ_H and the Nanshan phases Φ_N are quite possibly caused by the unreliable reference TOAs in the JBE parameters. Using the Nanshan phases as timing reference, the corrected X-ray phases Φ'_P show lower variation amplitude and remain almost constant over time with a change rate of $(-1.1 \pm 1.1) \times 10^{-7}$ period per day.

Based on the results above, we conclude that the distance of the X-ray and radio emission regions on the Crab pulsar does not show detectable secular changes, and the timing noises are not the result of any unique physical processes in the radio or X-ray radiation regions. In addition, the variation of the ISM is not the origin of Crab pulsar’s timing noises, which is consistent with the results obtained from the multi-frequency radio observations of PSR B1540–06 (Hobbs et al. 2010).

Acknowledgments

We appreciate Dr. Michael Smith, Lorenzo Natalucci, Craig Markwardt, Yuanyue Pan, Liming Song, Jinlu Qu, Li Chen, and Jian Li for their useful suggestions. This work is supported by the National Key Research and Development Program of China (2016YFA0400802), National Science Foundation of China (11233001, 11503027, and 11303069), the Strategic Priority Research Program on Space Science, and the Chinese Academy of Sciences, grant No. XDA04010300 and XDB23000000. This work is also partially supported by the Trainee Program of Qian Xuesen Laboratory of Space Technology. We thank the High Energy Astrophysics Science Archive Research Center (HEASARC) at NASA/Goddard Space Flight Center for maintaining its online archive service that provided the data used in this research.

REFERENCES

- Abdo, A. A., Ackermann, M., Ajello, M., et al. 2010, *ApJ*, 708, 1254
- Cordes, J. M., & Helfand, D. J. 1980, *ApJ*, 239, 640
- Cordes, J. M., 1993, in Phillips J. A., Thorsett S. E., Kulkarni S. R., eds, *Planets around Pulsars. Astron. Soc. Pac. Conf. Ser.*, Vol. 36, p. 43
- Edwards, R. T., Hobbs, G. B., & Manchester, R. N. 2006, *MNRAS*, 372, 1549
- Espinoza, C. M., Lyne, A. G., Stappers, B. W., & Kramer, M. 2011, *MNRAS*, 414, 1679
- Feigelson, E. D., & Babu, G. J. 2012, *Modern Statistical Methods for Astronomy*, UK: Cambridge University Press
- Garcia, J. A., McClintock, J. E., Steiner, J. F., Remillard, R. A., and Grinberg, V. 2014, *ApJ*, 794, 73
- Ge, M. Y., Lu, F. J., Qu, J. L., et al. 2012, *ApJS*, 199, 32
- Ge, M. Y., Yan, L. L., Lu, F. J., et al. 2016, *ApJ*, 818, 48
- Helfand, D. J., Taylor, J. H., & Manchester, R. N. 1977, *ApJ*, 213, L1
- Hobbs, G., Lyne, A. G., & Kramer, M. 2010, *MNRAS*, 402, 1027
- Hobbs, G. B., Edwards, R. T., & Manchester, R. N. 2006, *MNRAS*, 369, 655
- Jahoda, K., Markwardt, C. B., Radeva, Y., et al. 2006, *ApJS*, 163, 401
- Kaplan, D. L., Chatterjee, S., Gaensler, B. M., & Anderson, J. 2008, *ApJ*, 677, 1201
- Kuiper, L., Hermsen, W., Cusumano, G., et al. 2001, *A&A*, 378, 918
- Kuiper, L., Hermsen, W., Walter, R., & Foschini, L. 2003, *A&A*, 411, L31

- Lee Rodgers, J., & Nicewander, W. A., 1988, *AmSci*, 42, 59.
- Lyne, A. G., Pritchard, R. S., & Graham-Smith, F. 1993, *MNRAS*, 265, 1003
- Lyne, A., & Graham-Smith, F. 2012, *Pulsar Astronomy*, UK: Cambridge University Press, 2012
- Lyne, A., Graham-Smith, F., Weltevrede, P., et al. 2013, *Science*, 342, 598
- Molkov, S., Jourdain, E., & Roques, J. P. 2010, *ApJ*, 708, 403
- Nelson, J., Hills, R., Cudaback, D., & Wampler, J. 1970, *ApJ*, 161, L235
- Oosterbroek, T., Cognard, I., Golden, A., et al. 2008, *A&A*, 488, 271
- Rothschild, R. E., Blanco, P. R., Gruber, D. E., et al. 1998, *ApJ*, 496, 538
- Rots, A. H., Jahoda, K., & Lyne, A. G. 2004, *ApJ*, 605, L129
- Stairs, I. H., Lyne, A. G., & Shemar, S. L. 2000, *Nature*, 406, 484
- Wang, N., Manchester, R. N., Zhang, J., et al. 2001, *MNRAS*, 328, 855
- Yi, S. X., & Zhang, S.-N. 2015, *MNRAS*, 454, 3674
- You, X. P., Hobbs, G., Coles, W. A., et al. 2007, *MNRAS*, 378, 493
- Yuan, J. P., Manchester, R. N., Wang, N., et al. 2010, *ApJ*, 719, L111

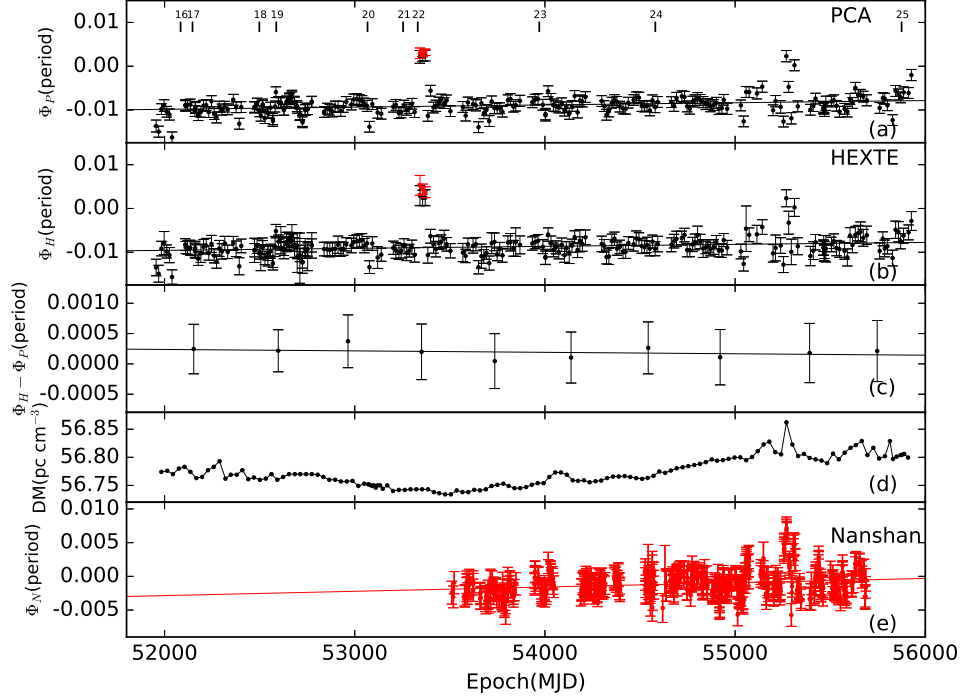


Fig. 1.— X-ray and Nanshan phases of the Crab pulsar from *RXTE*, and DM values in MJD 51955–55927. Panel (a) shows the X-ray phases of PCA, 2–60 keV. Panel (b) shows the X-ray phases of HEXTE, 15–250 keV. The error bars in Panels (a) and (b) include fitting and systematic uncertainties. Numbered tick marks in panel (a) indicate the time of glitches (Espinoza et al. 2011). Black points: the results obtained by FASEBIN. Red points: the results obtained by TEMPO2, see the details in Section 5.2; Panel (c) shows the phase lags between HEXTE and PCA. The data points are averaged over a time of about 400 days to show them tersely. Panel (d) shows the DM values, they are available from the web page <http://www.jb.man.ac.uk/pulsar/crab.html> (Lyne et al. 1993). Panel (e) is the Nanshan phases in MJD 53500–55693. In panels (a)-(e), the oblique solid lines are the fitting results.

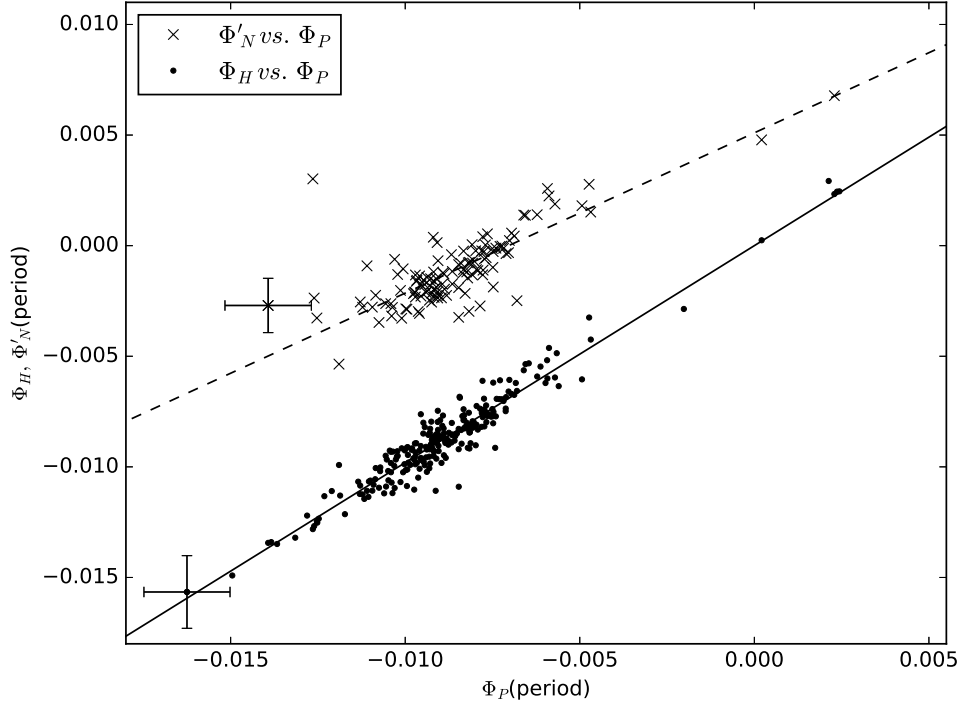


Fig. 2.— Correlations between the X-ray and interpolated Nanshan phases. The dots represent the correlation of X-ray phases from PCA and HEXTE. The cross marks represent the correlation of X-ray phases from PCA and interpolated Nanshan phases in MJD 53500–55693. The solid line is the fitting result of dots, while the dash line is the fitting result of cross marks. The typical errors are plotted to clearly show the correlations.

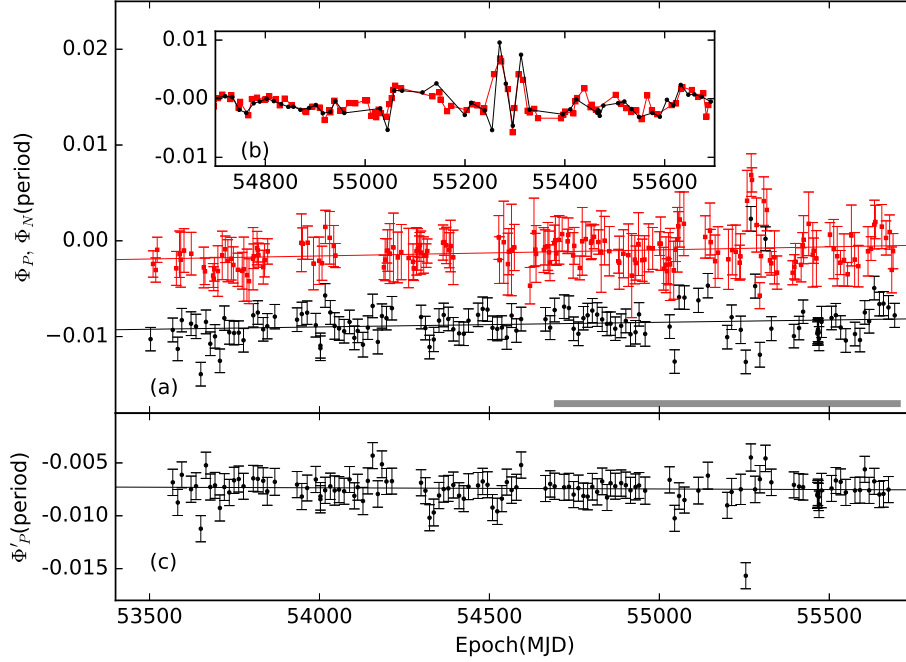


Fig. 3.— X-ray, Nanshan phases and corrected X-ray phases for PCA in MJD 53500–55693. Panel (a) shows the variations of X-ray phases from PCA (black dot points) and radio phases from Nanshan (red square points). The oblique solid lines are the fitting results. The inset (b) shows the X-ray and Nanshan phases in MJD 54700–55700 as marked with the gray belt in panel (a). The X-ray phases are shifted upward with 0.007 to compare them more clearly. The Nanshan phases are averaged in a time window of 1.5 days to show them tersely. Panel (c) shows the corrected X-ray phases from PCA.

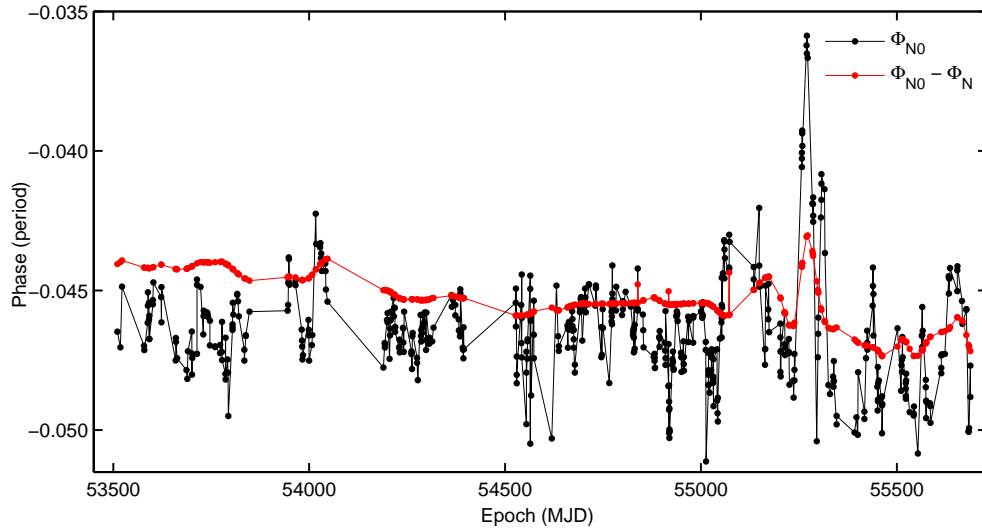


Fig. 4.— The Nanshan phases without de-dispersion and the phase differences between them and the Nanshan phase. Black points: the Nanshan phases without de-dispersion. Red points: the phase difference between Nanshan phases with and without de-dispersion. Φ_N is computed by using the steps (1)-(3) in Section 3.2, and in order to investigate the effect of DM, Φ_{N0} is computed by skipping the step (1).

Table 1: The change rates of X-Ray and radio phases

Instrument	MJD	Energy Band	Change Rate (10^{-7} period/day)	Intercept ^a (10^{-3} period)
PCA	51955–55927	2–60keV	5.0 ± 0.9	-8.8 ± 0.1
HEXTE	51955–55927	15–250keV	4.5 ± 0.9	-8.7 ± 0.1
PCA	53500–55693	2–60keV	4.8 ± 2.1	-9.0 ± 0.2
Nanshan	53500–55688	1540 MHz	6.3 ± 1.0	-1.6 ± 1.0
PCA ^b	53500–55693	...	-1.1 ± 1.1	-7.4 ± 0.1
HEXTE ^c	51955–55927	...	-0.2 ± 0.3	0.2 ± 0.04
PCA ^d	50129–52941	2–16keV	3.3 ± 2.0	...
PCA ^e	51955–55142	2–60keV	6.6 ± 1.3	...

Notes.

^a These intercepts correspond to the values at MJD 54000.

^b The parameters for X-ray phases from PCA corrected by data of the Nanshan Telescope.

^c The parameters for the phase lags between HEXTE and PCA.

^d The result from Rots et al. (2004).

^e The result from Ge et al. (2012).

Table 2: The correlation coefficients of the X-Ray and radio phases

Instrument	versus	Instrument	MJD	Slope	r
PCA	versus	HEXTE	51955-55927	0.98 ± 0.02	0.96
PCA	versus	Nanshan	53500-55693	0.72 ± 0.04	0.78